AUTOMATIC CALIBRATION OF DIGITAL CAMERAS USING PLANAR CHESS-BOARD PATTERNS

Valsamis DOUSKOS, Ilias KALISPERAKIS, George KARRAS
Department of Surveying, National Technical University of Athens, GR-15780 Athens, Greece
e-mails: mdouskos@googlemail.com, ilias_k@central.ntua.gr, gkarras@central.ntua.gr

KEY WORDS: Automation, Bundle, Calibration, Distortion, Extraction

ABSTRACT

A variety of methods for camera calibration, relying on different camera models, algorithms and a priori object information, have been reported and reviewed in literature. Use of simple 2D patterns of the chess-board type represents an interesting approach, for which several 'calibration toolboxes' are available on the Internet, requiring varying degrees of human interaction. This paper presents an automatic multi-image approach exclusively for camera calibration purposes on the assumption that the imaged pattern consists of adjacent light and dark squares of equal size. Calibration results, also based on image sets from Internet sources, are viewed as satisfactory and comparable to those from other approaches. Questions regarding the role of image configuration need further investigation.

1. INTRODUCTION

Camera calibration constitutes a fundamental task in photogrammetry and computer vision. A significant number of methods for camera calibration have been reviewed in literature (Clarke and Fryer, 1998; Salvi *et al*., 2002; Villa-Uriol *et al*., 2004). Approaches differ in various respects: they can involve single images or multi-image configurations; different camera models are adopted; the image features may be points but also lines (e.g. Grammatikopoulos *et al.*, 2007); linear and non-linear algorithms are used; targeted 3D or 2D test-fields are usually employed but camera calibration is also practicable with no a priori object information. Self-calibration is indeed feasible with simple image correspondences among frames, yet the participation of control points produces more robust calibration results, in closer agreement with object space constraints. Further, in practical close-range photogrammetric projects camera pre-calibration through appropriate image networks may often be preferable (Remondino and Fraser, 2006).

In this context, methods for estimating camera parameters rely typically on targeted test-fields and correspondences between targets and their images on one or more frames. For multi-image configurations, precise 3D test-fields can be replaced by simple 2D patterns, typically of a chess-board type. If indeed a camera should, ideally, be automatically calibrated solely from image sets taken rapidly with unknown exterior orientation (Fiala and Shu, 2005), a further advantage of such patterns is the fact that their high contrast and regularity facilitate automation based on feature extraction tools.

Several freely available algorithms exist for estimating interior and exterior orientation parameters based on chess-board patterns imaged from different points of view. These have been essentially inspired by the 'plane-based calibration' approach (Sturm and Maybank, 1999; Zhang, 1999) which is a process relying on the computation of homographies between a plane with known metric structure and its images. These 2D projective transformations yield a system of linear equations in the camera parameters, hence the initialisation step results in a closed-form solution for these parameters, in which lens distortion is generally not included (Sánchez et al., 2006). This phase is usually followed by a non-linear refinement step, based on the minimization of the total reprojection error.

Among functional tools presented in this context, Bouguet's *Camera Calibration Toolbox for Matlab*® (also implemented in C++ and included in the Open Source Computer Vision library distributed

by Intel) is probably best known. The initialisation step includes manual pointing of the four chess-board corners on all images and knowledge of the number of nodes per row and column. Node locations can thus be first approximated and then identified with sub-pixel accuracy by a point operator. If lens distortion is strong, one may need to supply approximations for its coefficients. Initial values are provided by the plane-based calibration algorithm, while an iterative adjustment provides a final solution for camera and pose parameters. Other variations with higher degree of automation (see the Bouguet website), some of which are 'add-ons' to this toolbox, require special target types, patterns with odd and even number of corners in the two directions, or assumptions about the magnitude of lens distortion and the demand that the full calibration pattern is visible on the images.
Recently, a camera calibration toolbox has become freely available from the Institute of Robotics & Mechatronics, DLR, Germany (see *DLR CalDe – DLR CalLab* website). The calibration pattern does not need to be fully imaged, hence the whole format can be exploited for estimating lens distortion. The operation is fully automatic if the chess-board contains three circular targets in its centre, else such points must be given manually. After a first solution, a tool is provided to identify and remove erroneously detected corners by setting a threshold for residuals. This procedure has not been automated since such decisions are regarded as depending to a great extent on the particular cameras.
Our contribution presents an implemented automatic algorithm for the exclusive purpose of camera calibration, in the sense that exterior orientation is here irrelevant. This is achieved using image sets of typical chess-board patterns (alternating light and dark squares of equal size), which is the sole a priori information needed. Only those extracted image points are kept which may be ordered in two groups of lines referring to the main orthogonal directions on the object plane. Due to the regularity of the pattern, establishing point correspondences among views is then a trivial task, albeit possibly involving object systems which differ in in-plane rotation and translations. Yet the fact that homologue image points do not necessarily refer to the same physical point of the pattern affects only the exterior orientations. Initial values are found from the image vanishing points, and a final estimation for camera parameters is obtained from bundle adjustment. The process is described in the next sections, where calibration results from different cameras are also presented and evaluated. It is to note that in the following 'reasonable' images are assumed, taken indeed for calibration purposes (the pattern occupies a substantial part of the frames, no objects interfere with the pattern etc.).

2. CAMERA CALIBRATION ALGORITHM

2.1 Initialisation step

2.1.1 Corner extraction. With parameters chosen after some tests, the Harris corner operator with sub-pixel accuracy, made available by Bouguet in his website, is applied to grayscale images with equalized histograms. Image standard errors of bundle adjustments have corroborated the assertion that the corners are extracted to an accuracy of ~0.1 pixel. Indeed, in all experiments this phase has supplied good results, by extracting practically all pattern nodes and rather few redundant points. Indications for the satisfactory performance of the sub-pixel Harris operator in case of chess-board patterns are also found in Ouyang *et al*. (2005).

2.1.2 Point ordering. After extraction of feature points on an image, the medians of their x, y co-ordinates are calculated. These will normally indicate a point close to the centre of the chess-board pattern. The median is preferred against the mean value due to its lower sensitivity to the presence of 'noisy points' outside the chess-board. The point selection and ordering algorithm is initialized by choosing the closest feature point as 'base point' B.
All extracted points around B in a window of size equal to ⅓ of the image size are calculated and sorted according to distance from it. Assuming that B is indeed a valid node, the principal directions of the pattern must now be identified by avoiding points not corresponding to pattern nodes but also points on chess-board diagonals. The linear segment *s* from 'base point' B to the nearest extracted

point is formed. Identification of the main directions succeeds by comparing the grey values of the pixels on either side of *s*. Thanks to the chess-board pattern, if this segment *s* indeed belongs to one of the principal directions, a large difference in grey values must occur between the two sides of *s*. The representative grey value on either side is calculated from a sample along a line parallel to *s*, with length equal to ⅓ of the length of *s* and midpoint distanced half the length of *s* away from the midpoint of *s*. If the difference between the mean grey values of these samples on either side of *s* is found to exceed by more than 3 times the overall standard deviation of image grey values, then this segment *s* is regarded as belonging to one of the principal directions.

This is repeated for the next 7 closest points around B. If the other main direction (i.e. perpendicular to the first on the chess-board) is also found, these two segment lengths and directions are stored as initial reference values, and the algorithm continues to identify the rows and columns of the pattern. If it is not possible to establish both directions, then this 'base point' B probably does not represent a chess-board node, or there are few neighbouring points around it. Thus, the process is resumed by selecting as new 'base point' B that next closest to the 'median point'. This procedure is repeated until both principal directions have been fixed.

A similar search evolves for the next points of these two lines. Using the stored segment length and angle of the respective main direction, the position of the next point on the line is anticipated. The algorithm searches within a small region, defined by thresholds in segment length and angle, around this estimated point position to locate extracted feature points. If a point is found, it is considered as part of the same line (optionally the grey-value criterion may also be used here, yet for all practical tests carried out this has not been necessary). This point becomes now the new 'base point' for the next search, while values for segment length and direction are updated with the new segment. Next segments define new search lengths and directions. It is noted that – contrary to approaches where point locations are estimated by means of the four corner points – here the effect of lens distortion on the directions defined by neighbouring nodes on a line is regarded as negligible.

It is not indispensable to identify all individual nodes. In case of a missing node, the position of the next one is estimated and an acceptable extracted point is again searched for. When three successive 'missing points' have been encountered, it is assumed that all line points have been located and the search is halted. This is repeated for locating all points of the 'perpendicular' line. Lines which have less than 4 points are regarded as unreliable and a 'gap' is considered in their place.

Next, from the central point of this line using the 'perpendicular' direction and the corresponding segment length, a point of the next 'parallel' line is estimated. If a point is found, the same process is continued. Otherwise, starting from points next to this central point, corresponding points on the 'parallel' line are searched for. If it is not possible to locate points on this line, a 'gap 'is set in its place and the algorithm seeks after a point of the next 'parallel' line. When three successive 'gaps' are met, the algorithm accepts that there are no further detectable lines in this direction. The process continues with a similar search for converging image lines (parallel chess-board lines), guided as before by local segment length and direction.

After the detection process for chess-board lines is terminated, these are ordered. The line through the original 'base point' which forms smaller angle with the image x-axis fixes the group of 'rows'; the other line fixes the 'columns'. Rows and columns are sorted according to the coordinate of their intersection with the respective image axis (y for rows, x for columns). It is stressed that, as a basic precaution, only points which belong to both a row and a column are accepted as valid chess-board corners. This permits to discard 'outliers', i.e. points (particularly outside the pattern) which might happen to be nearly collinear with a chess-board line and their distance from some point of the line falls within the local tolerance of segment length. In Fig. 1 two examples illustrate the three basic steps of point extraction, line formation and final selection of chess-board nodes.

2.1.3 Point correspondences. The final outcome of this step is a set of points characterized by the number of the respective chess-board row and column with which they are associated. The lower row appearing on an image is row 1 and is arbitrarily associated with the object X-axis. The column to the far left is column 1 and associated with the object Y-axis. Thus, the point belonging to these

two lines is point (1,1) of this image and is associated with the origin (point 1,1) of the chess-board XY system. If this point does not actually appear on an image or has not been detected, the adjacent node detected on this image is numbered accordingly, e.g. (2,1) or (1,2) etc. The process is repeated for all images. Hence, thanks to the symmetric nature of the pattern, it may be assumed that point correspondences among frames as well as correspondences with the chess-board nodes have been established. This provides an answer to the problem of correspondences, which is seen as the most difficult part in automatic camera calibration and is often solved manually (Fiala and Shu, 2005).

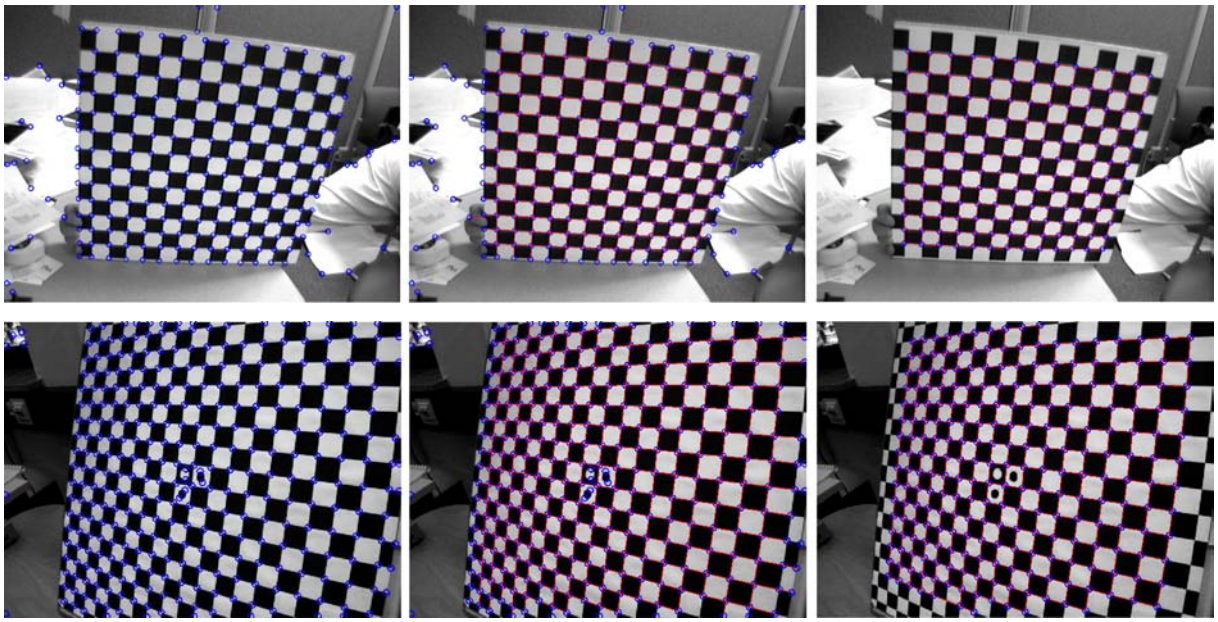

Figure 1. Initially extracted points (left), formed lines (centre), final nodes (right).

Clearly, the exterior orientation (pose) of images is here irrelevant. Images refer to their own object systems which may differ by in-plane translation and rotation. Consequently, point correspondences among views established above will not necessarily refer to identical physical points of the pattern. But this can be tolerated thanks to the symmetry of the chess-board. Generally speaking, for camera calibration with 2D object control it is the perspective distortions of images which primarily matter, i.e. their relation to the symmetric planar object and not to a fully fixed system in object space.
Yet, it must be noted that this process (e.g. images taken from different sides of the pattern may be treated as taken from the same side) has its effect on the ray intersection angles in self-calibration. If no ground control is used, this will be reflected in the precision of interior orientation parameters. However, since our approach presupposes equal pattern squares, object coordinates (in an arbitrary scale) can be introduced in bundle adjustment. If these are treated as error-free or highly weighted, the arbitrary choice of object systems is not expected to affect significantly the precision of camera calibration. On the other hand, orthogonal roll angles loosen correlations between interior and exterior orientation parameters (Remondino and Fraser, 2006). Our approach is inherently incapable of recognizing such rotations – a price paid when using plain chess-board patterns without special targets for the orientation of the object system. Interchange of X and Y object axes in some images might be a possible answer to this. In a first test this has weakened significantly the largest correlations (those of y_o with rotations ω and κ) at the expense of an increase of the smaller correlations (of y_o with ϕ and of x_o with ω and κ). This, too, is a point for further investigation.

2.1.4 Initial values. Instead of the linear solution of plane-based calibration, the approach adopted here relies on the two principal vanishing points (VP) of the images. These are found by line-fitting adjustment to nodes ordered in pencils of converging lines. In each direction, initial estimates of VP locations are obtained from the two lines with >3 points forming the largest angle. If the distance of

a VP from the image centre exceeds by more than 40 times the size of the image format (equivalent to a rotation angle ~1.5° for a moderately wide-angle lens), this VP is considered at infinity. If both VPs are finite, their locations are refined in a single adjustment, in which coefficients of radial lens distortion are also included in the unknowns. Using diagonals with >3 points, the VP of the diagonal direction which falls between the two principal VPs is also included as an unknown to enforce the vanishing line constraint. In case one VP is finite, it is estimated from all participating lines along with the radial distortion coefficients.
Assuming the principal point at the image centre, camera constant c and image rotation matrix can be found from the two principal VPs of each participating image according to Karras *et al.* (1993). The estimations of c and the distortion coefficients with the smallest standard errors (σ_c is estimated through error propagation) will be used as initial values in the bundle adjustment. If one of the VPs is assumed at infinity, the corresponding out-of-plane rotation (ω or ϕ) is set to zero, the other is found using the above-mentioned initial value for c; estimation of image roll κ is trivial. Finally, the largest dimension in X seen in all images (arbitrarily scaled) is used for approximating the camera altitudes. The planimetric position of the projection centre in the object system of each image may then be estimated from the image coordinates of the origin (point 1,1). If this latter point has not been detected on an image, its location is approximated by the intersection of row 1 with column 1.

2.2 Bundle adjustment

Finally, an iterative bundle adjustment is carried out for a final estimation of camera geometry parameters. Since the algorithm also functions in a pure self-calibration mode (no object control) some results are given for comparison in the following section. Yet the main results presented are based on control points with uncertainty set here to 0.1‰ of the chess-board dimension. Besides camera constant c and principal point location (x_o, y_o) the adopted camera model also includes image aspect ratio and the four coefficients k_1, k_2 for radial symmetric lens distortion and p_1, p_2 for decentering distortion (Brown, 1966). Image pixels are treated as rectangular. However, as also seen in our experiments, decentering distortion in current digital cameras is mostly negligibly small compared to sensor quantization, and hence a possible source of instability (Zhang, 1999); image aspect ratio is also mostly insignificant (Remondino and Fraser, 2006). In the next section, results for aspect ratio are only given for the purposes of comparison with results from other algorithms.

3. PRACTICAL EVALUATION

Tests with two cameras were performed using different image sets for each camera.
• ***Camera 1.*** Three sets of 640×480 images, presented in Fig. 2, were used for the first camera. Set 1 (with 9 images) is 'weak', since in most images the pattern covers a relatively small image area. Set 2 includes only 4 images, which however have a better scale. The third set has 9 images similar to those of set 2 and represents a much stronger geometry. Results are seen in Table 1, in which σ_o stands for the standard error of the adjustment.

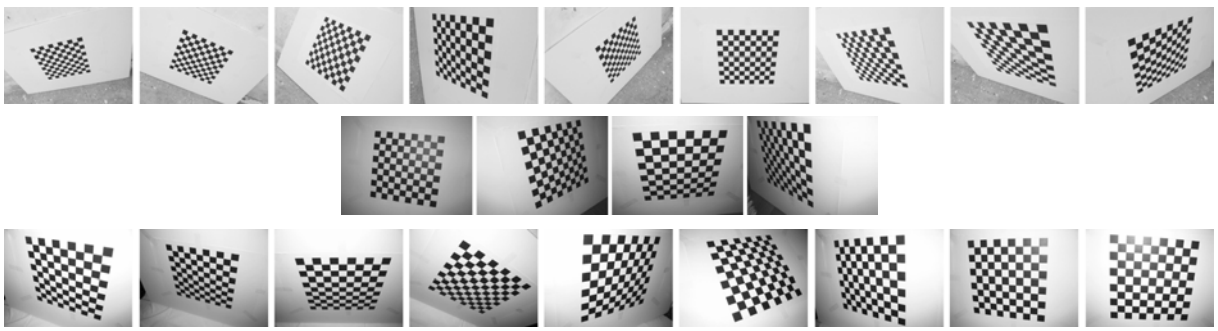

Figure 2. Image sets for Camera 1 (above: set 1, middle: set 2, below: set 3).

Table 1. Calibration results for Camera 1 (*italics: without use of control points*)

Sets	σ_o (pix)	c (pix)	x_o (pix)	y_o (pix)	$k_1\times10^{-7}$ (pix^{-2})	$k_2\times10^{-13}$ (pix^{-4})
1	0.16	675.22 ± 0.42	–4.79 ± 0.29	0.70 ± 0.35	-4.003 ± 0.077	9.644 ± 0.896
2	0.15	671.28 ± 0.56	–3.63 ± 0.27	–0.44 ± 0.37	-4.107 ± 0.058	10.508 ± 0.461
3	0.14	670.55 ± 0.26	–4.41 ± 0.17	0.47 ± 0.20	-4.087 ± 0.049	9.798 ± 0.473
3	*0.10*	*670.10 ± 0.23*	*–6.63 ± 0.43*	*0.56 ± 0.45*	*-4.190 ± 0.049*	*10.201 ± 0.401*

The principal point locations are very close to each other in all three sets, while the radial distortion curves are practically the same (differences are well below 1 pixel at image corners). However, the camera constant estimated by set 1, in which image coverage is small, shows a difference of about 0.7%, while the radial distortion has the smallest precision. Despite its few images, set 2 produces results close to those of set 3, albeit with higher standard errors. The standard errors provided by the much stronger geometry of the last set are satisfactory. It is noted that even the results from self-calibration without the use of control points (in italics in Table 1) are also close to those when using control, but with a clearly smaller precision in the location of the principal point.

• ***Camera 2.*** Two sets of 648×486 images, which are shown in Fig. 3, have been used for the second camera. Both sets include 7 images and are regarded as representing satisfactory configurations as regards image coverage, image scale and scale variations, as well as differences in perspective distortions. Results are given in Table 2.

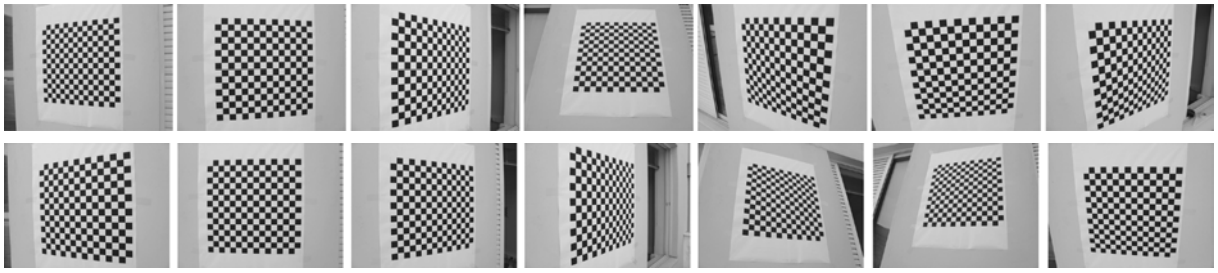

Figure 3. Image sets for Camera 2 (above: set 1, below: set 2).

Table 2. Calibration results for Camera 2 (*italics: without use of control points*)

Sets	σ_o (pix)	c (pix)	x_o (pix)	y_o (pix)	$k_1\times10^{-7}$ (pix^{-2})	$k_2\times10^{-12}$ (pix^{-4})
1	0.14	643.66 ± 0.22	3.71 ± 0.15	3.99 ± 0.13	–5.149 ± 0.051	1.553 ± 0.060
2	0.13	642.61 ± 0.24	2.44 ± 0.16	2.73 ± 0.14	–5.277 ± 0.058	1.694 ± 0.077
1	*0.05*	*643.96 ± 0.10*	*2.57 ± 0.47*	*1.18 ± 0.40*	*–4.964 ± 0.030*	*1.350 ± 0.030*
2	*0.05*	*643.92 ± 0.11*	*2.88 ± 0.48*	*2.77 ± 0.44*	*–5.022 ± 0.032*	*1.391 ± 0.037*

The repeatability of calibration for these image sets is high, even without the involvement of control points. Besides, values for all parameters of this camera from previous bundle adjustments with 3D control fall within the range of Table 2. The fact that the standard error σ_o trebles when control is introduced may be attributed to deviations of the pattern from planarity due to its large size.

• ***Image set of Bouguet***. Our algorithm has also been applied to the 20 images of the set given by J.-Y. Bouguet in his web site (one of them is seen in the first row of Fig. 1). The results are presented in Table 3. Included are also those given by Bouguet, in which σ_o stands for the 'reprojection error', while distortion coefficients have been reduced by corresponding powers of the camera constant to become comparable with our results. Values for the coefficients of decentering distortion are not included since they are insignificant compared to their standard errors (especially p_1). It is seen that the results are fully compatible (in fact even when no ground control is used), with distortion curves being practically coincident.

Table 3. Calibration results for the Bouguet image set (*italics: without use of control points*)

Results	σ_o (pix)	c_x (pix)	c_y (pix)	x_o (pix)	y_o (pix)	$k_1\times10^{-7}$ (pix^{-2})	$k_2\times10^{-13}$ (pix^{-4})
Bouguet	0.12	657.46 ± 0.32	657.95 ± 0.34	–16.86 ± 0.65	–2.57 ± 0.59	–5.872 ± 0.057	6.489 ± 0.527
	0.10	657.78 ± 0.11	658.17 ± 0.12	–16.68 ± 0.10	–4.21 ± 0.11	–5.972 ± 0.020	7.282 ± 0.183
	0.09	*658.15 ± 0.17*	*658.74 ± 0.11*	*–18.45 ± 0.50*	*–4.07 ± 0.49*	*–6.036 ± 0.020*	*7.458 ± 0.168*

• ***Image sets of DLR***. Further, the algorithm has also been used with two sets of ten 780×580 images (one of them seen in the lower row of Fig. 1) of the *DLR CalDe – DLR CalLab* website. These have been acquired with a stereo-camera treated here as two independent cameras (I and II). It is noted that these lenses have stronger radial distortion, and also that the pattern is only partly recorded in some images. Results are presented in Table 4, where also results from the DLR software in single-image mode are included (here again σ_o stands for the 'reprojection error', while distortion coefficients have been accordingly reduced). This software does not supply standard errors of parameters.

Table 4. Calibration results for the DLR image set (*italics: without use of control points*)

Results	σ_o (pix)	c_x (pix)	c_y (pix)	x_o (pix)	y_o (pix)	$k_1\times10^{-7}$ (pix^{-2})	$k_2\times10^{-13}$ (pix^{-4})
(I) DLR	0.18	727.51	726.54	–16.13	–1.28	–3.824	3.524
(I)	0.16	726.12 ± 0.17	725.45 ± 0.17	–16.20 ± 0.13	–6.89 ± 0.13	–3.889 ± 0.018	4.017 ± 0.087
(I)	*0.13*	*727.05 ± 0.23*	*726.63 ± 0.26*	*–15.48 ± 0.47*	*0.24 ± 0.55*	*–3.911 ± 0.023*	*4.008 ± 0.096*
(II) DLR	0.15	731.79	730.60	–20.01	–4.50	–3.990	4.335
(II)	0.14	731.44 ± 0.15	730.37 ± 0.15	–20.51 ± 0.11	–5.66 ± 0.11	–3.969 ± 0.017	4.357 ± 0.085
(II)	*0.12*	*731.24 ± 0.19*	*731.28 ± 0.24*	*–18.83 ± 0.42*	*–2.34 ± 0.51*	*–3.948 ± 0.020*	*4.453 ± 0.090*

Our results are not directly comparable to those from the DLR software since when using it we had to discard 60 to 70 erroneous image points near the edges to obtain a reasonable reprojection error. However, with the exception of y_o in the first camera the calibration results stand in rather good agreement, with coincident distortion curves. When no control is used, a deviation of a few pixels occurs in the principal point location (mainly in y_o).

• ***Image set of Zhang***. Last, the algorithm was used with the 5 images (640×480) from the website of Zhang. In this case the corners of the patterns are not equally spaced, i.e. they are unsuitable for our algorithm. Yet their distances fall within the threshold used in our approach and, since the full pattern is recorded, it was possible to establish correspondences automatically. Control point coordinates were given. Table 5 includes the results of Zhang (1999) with the omission of skewness.

Table 5. Calibration results for the Zhang image set (*italics: without use of control points*)

Results	σ_o (pix)	c_x (pix)	c_y (pix)	x_o (pix)	y_o (pix)	$k_1\times10^{-7}$ (pix^{-2})	$k_2\times10^{-13}$ (pix^{-4})
Zhang	0.33	832.50 ± 1.41	832.53 ± 1.38	–16.04 ± 0.71	33.41 ± 0.66	–3.290 ± 0.043	3.955 ± 0.520
	0.23	832.76 ± 1.42	833.09 ± 1.40	–16.45 ± 0.47	35.29 ± 0.41	–3.326 ± 0.072	4.064 ± 0.625
	0.15	*832.39 ± 1.19*	*831.98 ± 1.38*	*–9.76 ± 6.60*	*41.39 ± 5.51*	*–3.360 ± 0.130*	*4.787 ± 0.802*

The results are indeed compatible in all parameters, though with large standard errors attributed to the weak configuration of these five images from a normal-angle lens. Due to this, the solution from pure self-calibration (no ground control) is obviously quite unreliable.

4. CONCLUDING REMARKS

An approach has been presented for the automatic multi-image calibration of cameras from images of 2D chess-board patterns, under the single assumption that these consist of adjacent equally sized squares. Calibration results, including those using image sets from different Internet sources, are regarded as satisfactory and comparable to results from other approaches for camera calibration with planar objects. Of course, this presupposes that 'reasonable' image sets (in quality, pattern coverage and number) are used, with significant differences in perspective to constitute strong configurations. In such instances it appears that even the total absence of control points may produce usable results. Exterior orientation is here irrelevant due to the symmetry of the pattern, which interferes with the strength of ray intersections in bundle adjustment. Further, images with orthogonal roll angles cannot be treated as such. This raises certain questions regarding the precision of results, particularly as regards principal point location, whose variability is generally regarded as high compared to other camera parameters (Ruiz *et al.*, 2002). With camera calibration from 2D patterns being indeed an attractive and simple approach yet with high potential, such aspects need to be further investigated.

References

Bouguet J.-Y., *Camera Calibration Toolbox for Matlab*, http://www.vision.caltech.edu/bouguetj/calib_doc/

Brown D.C., 1966. Decentering distortion of lenses. *Photogrammetric Engineering*, 32(3), pp. 444-462.

Clarke T.A., Fryer J.G., 1998. The development of camera calibration methods and models. *The Photogrammetric Record*, 16(91), pp. 51-66.

DLR CalLab – CalDe Software, http://www.dlr.de/rm/desktopdefault.aspx/tabid-1524/

Fiala, M., Shu, C., 2005. *Fully Automatic Camera Calibration Using Self-Identifying Calibration Targets*. Technical Report 48306/ERB-1130, National Research Council Canada, pp. 26.

Grammatikopoulos L., Karras G., Petsa E., 2007. An automatic approach for camera calibration from vanishing points. *ISPRS Journal of Photogrammetry and Remote Sensing*, vol. 62, pp. 64-76.

Intel OpenCV Computer Vision Library (C++), http://www.intel.com/research/mrl/research/opencv/

Karras G., Patias P., Petsa E., 1993. Experiences with rectification of non-metric digital images when ground control is not available. *Proc. XV International CIPA Symposium*, Bucharest (unpaginated).

Ouyang C., Wang G., Zhang Q., Kang W., Ding H., 2005. Evaluating Harris method in camera calibration. *27th IEEE Engineering in Medicine & Biology An. Conf.*, Shanghai, September 1-4, pp. 6383-6386.

Remondino F., Fraser C., 2006. Digital camera calibration methods: considerations and comparisons. *International Archives of Photogrammetry, Remote Sensing and the Spatial Sciences*, 36(5), pp. 266-272.

Ruiz A., López-de-Teruel P.E., García-Mateos G., 2002. A note on principal point estimability. *Proc. 16th Int. Conf. Pattern Recognition (ICPR '02)*, 11-15 August, Quebec, Canada, vol. 2, pp. 304- 307.

Salvi J., Armangué X., Batlle J., 2002. A comparative review of camera calibrating methods with accuracy evaluation. *Pattern Recognition*, 35, pp. 1617-1635.

Sánchez J.A., Destefanis E.A., Canali L.R., 2006. Plane-based camera calibration without direct optimization algorithms. *IV Jornadas Argentinas de Robótica*, Córdoba, 16 -17 November.

Sturm P.F., Maybank S.J., 1999. On plane-based camera calibration: a general algorithm, singularities, applications. *IEEE Conf. Computer Vision & Pattern Recognition (CVPR'99)*, Fort Collins, USA, pp. 432-37.

Villa-Uriol M.-C., Chaudhary G., Kuester F., Hutchinson T. C., Bagherzadeh N., 2004. Extracting 3D from 2D: selection basis for camera calibration. *IASTED Computer Graphics & Imaging*, Kauai, USA, pp. 315-321.

Zhang Z., 1999. Flexible camera calibration by viewing a plane from unknown orientations. *Int. Conf. on Computer Vision (ICCV'99*), Corfu, Greece, pp. 666-673.

Zhang Z., *A Flexible New Technique for Camera Calibration*, http://research.microsoft.com/~zhang/Calib/